Journal of Materials Processing Technology 243 (2017) 40–47

Contents lists available at ScienceDirect

Journal of Materials Processing Technology

journal homepage: www.elsevier.com/locate/jmatprotec

Optimization of wire feed for GTAW based additive manufacturing

Haibin Geng[a,b], Jinglong Li[b,*], Jiangtao Xiong[b], Xin Lin[a], Fusheng Zhang[b]

[a] State Key Laboratory of Solidification Processing, Northwestern Polytechnical University, Xi'an 710072, PR China
[b] Shaanxi Key Laboratory of Friction Welding Technologies, Northwestern Polytechnical University, Xi'an 710072, PR China

ARTICLE INFO

Article history:
Received 13 September 2016
Received in revised form
22 November 2016
Accepted 23 November 2016
Available online 24 November 2016

Keywords:
Wire and arc additive manufacture
Wire melting behavior
Droplet transfer
Layer appearance
Layer start position

ABSTRACT

The problem of deposition accuracy is encountered during gas tungsten arc welding (GTAW) based additive manufacturing when wire is fed in side direction. A mathematical model was developed to calculate the wire flying distance in arc zone, according to which displacement compensation was designed to ensure the size accuracy. When arc length was 5 mm and vertical distance of wire tip to tungsten electrode was larger than 3 mm, the horizontal distance between melting wire tip and axis of tungsten electrode was 3.5 mm. The displacement compensation was verified to be effective by forming cross-angle. The model can also be used to achieve bridging transfer, which is beneficial for smooth layer appearance.

1. Introduction

Compared with laser and electron beam additive manufacturing, wire and arc additive manufacturing (WAAM) has unique superiorities in shape deposition efficiency and product cost. Baufeld et al. (2011) thought that it is suitable for near net shape forming large sized components. The low investment cost of equipment and the popularization of arc welding make WAAM the most promising techniques in industrial application. The separate processes of energy input and materials input during gas tungsten arc welding (GTAW) are beneficial for smooth layer appearance, especially for aluminium and its alloys. Wang and Kovacevic (2001) indicated that cleaning action of the cathode plays a crucial role during GTAW based additive manufacturing aluminium alloy, which helps to remove the oxide formed on layer surface. Such phenomenon allows the molten metal to wet the substrate smoothly and helps to maintain the stable arc on the molten pool surface by providing ionized Al vapor as arc medium.

For aluminium and its alloy, cleaning action of the cathode is necessary, but that has more significant influence on materials input and arc stability during gas metal arc welding (GMAW) or cold metal transfer (CMT) based additive manufacturing. Discontinuous materials input and arc blow are furtherly exacerbated by thermal pinch effect of aluminium alloy. These go against forming smooth layer appearance. GTAW based WAAM is more suitable for additive manufacturing aluminium and its alloy. To obtain uniform layer size and appearance, heat input should be regulated during layer upon layer deposition because of the heat accumulation effect. During GTAW based WAAM process, heat input adjustment does not change arc length and the deposition rate can be controlled independently by adjusting wire feed speed, which mean that the two separate processes of energy input and materials input make WAAM control easier by comparing with GMAW or CMT based additive manufacturing. However, GTAW based WAAM usually suffers deposition accuracy problem at the start position, where the as-deposited weld bead would shift a little from the preset position causing by wire feed in side direction. Such wire feed manner tends to produce gap defect in cross- or T-type structure and lead to deposition failure. So far this problem has not drawn any researchers' attention, but in WAAM process, it is quite important to ensure the final structure accuracy.

Gap defects occurred in a deposited structure are shown in Fig. 1, where a bridge was deposited to connect two cylinders. The gap appeared at the arc striking position, which implies layer start position shift. Furthermore, such defect cannot be corrected by the succeeding layer deposition.

Wire feed manner design could be one of the methods to eliminate the defect. However, it is usually kept unchanged (i.e., side feeding with fixed angle and height) during process parameters optimization. The nature of WAAM is shaping process with short-range free flow in molten pool, continuity and stability of material input will contribute to achieve smooth and flat layer appearance, which is a constrain to wire feed adjusting. If wire feed manner is varied to eliminate the gap defect, the deposition process may

* Corresponding author.
E-mail address: lijinglg@nwpu.edu.cn (J. Li).

http://dx.doi.org/10.1016/j.jmatprotec.2016.11.027
0924-0136/

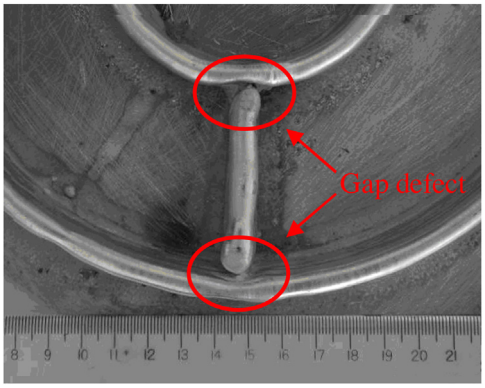

Fig. 1. Gap defects resulted by start position shift when depositing "T type" structure.

become unstable and result in surface appearance defects, such as humping and gouging.

So wire feed manner can not be set arbitrarily because it has relation with layer appearance in manner of materials input. That is, surface quality is the premise of layer size accuracy control. The surface quality is determined by the matched heat input and materials input. Ouyang et al. (2002) fabricated 5356 aluminium alloy cylindrical parts with perfectly acceptable surface quality using GTAW method. A machine vision sensor was used to monitor and control the arc length, and the height of deposited layer is regulated by optimizing travel speed in order to match heat input to preset wire feed manner. Wire feed manner is denied to be varied, or the regulation should be recalibrated.

In the situation without feedback control, the matched heat input to materials input can be obtained by process optimization on the premise of stable materials input in manner of bridging transfer. By using this method, Wang et al. (2013) deposited two Ti-6Al–4V straight walls with 6.8 mm thick using GTAW based WAAM. As expected, the wall surface showed uniform fluctuation resulted by layer by layer deposition. However, the accuracy of start position was not mentioned. Baufeld et al. (2009) deposited cylindrical and rectangular parts, in which the weld gun travelled along closed path and did not encounter the layer size accuracy problem. They made efforts on process optimizations to ensure consistent layer appearance, in which the wire feed manner was kept unchanged. If only to obtain smooth and consistent layer appearance, the above mentioned process optimization is workable. However, it can not be achieved when considering both stable layer formation and structure accuracy. Thus, it is reasonable to set wire feed manner as a variable during process optimization, i.e., this problem would be readily solved by consider both the start position shifting and stable forming process (For wire feed, it means stable materials input).

GTAW based additive manufacturing of aluminium alloy is conducted, which focuses on layer size accuracy and droplet transfer behavior from the view point of wire feed manner regulation. To avoid start position shift happening and ensure smooth layer appearance, wire feed manner is set as control variable during process optimization. A mathematical model is developed to calculate the wire flying distance in arc zone, according which displacement compensation at the arc striking position could be set. Besides, threshold condition of bridging transfer is also developed from this model.

2. Experimental procedures

A GTAW welding machine (EWM, Tetrix 521 Synergic AC/DC) with wire feeder was used for the experiment. Fig. 2 shows the wire feeding unit and the related parameters about wire feed manner.

Fig. 2b defines the height of wire rotation axis to substrate, h, of which the increment Δh denotes the wire vertical adjusting tolerance and θ the wire feed angle. Both h and θ will be cooperated to determine droplet transfer mode: bridging or globular transfer.

A computer numerical control (CNC) machine tool with four axes was used as manipulator, where welding torch was installed on the moving arm in downward position. Arcing and wire feeding are started simultaneously by integrating arc striking, extinguishing and wire feeding commands into CNC program. The experiment was conducted using a Φ1.2 mm 5A06 aluminium alloy wire, which was deposited on the substrate with dimension of 300 × 200 × 15 mm. The wire feed direction is always in front of the welding arc. A water-cooling backing plate was used to extract heat from the substrate. The deposition direction was unaltered and all started at the same position to facilitate comparing the shift of weld bead start position. Argon (99.99%) was used as shielding gas. Rectangular pulse AC power mode was adopted with peak and background current set as 160 A and 100 A respectively, and the pulse frequency was set as 50 Hz. The other related welding power supply parameters are listed in Table 1. In addition, diameter of tungsten electrode used in all experiments was Φ3.2 mm, wire feed speed was 2 m/min, and the travel speed was 300 mm/min. The droplet transfer is observed using high speed video camera (Phantom V310). Frame number of high-speed camera is 4000 fps.

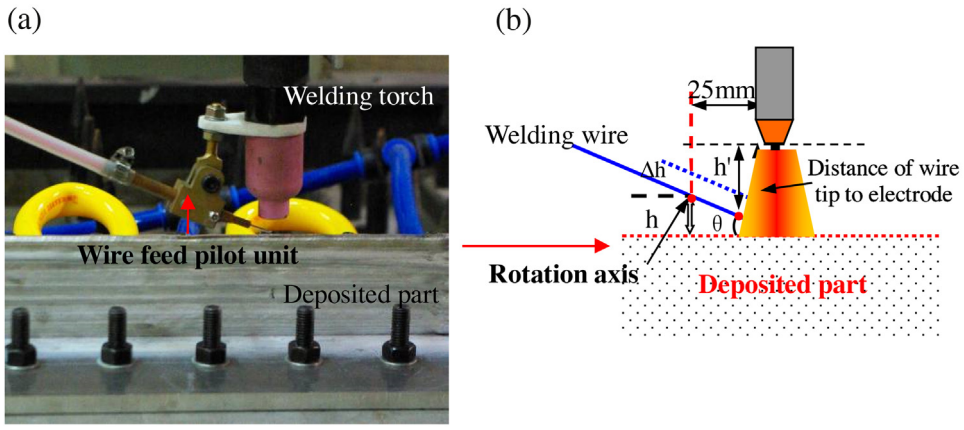

Fig. 2. Wire feed unit showing (a) site photo and (b) schematic illustration of the parameters.

Table 1
Power supply parameters applied in this experiment.

Peak current time (s)	Duty ratio	Pulse frequency (Hz)	Down slop time (s)	Pre-flow time (s)	Post-flow time (s)	Gas flow (L/min)	Arc length (mm)
0.01	0.5	50	1.8	1.5	4	10	5

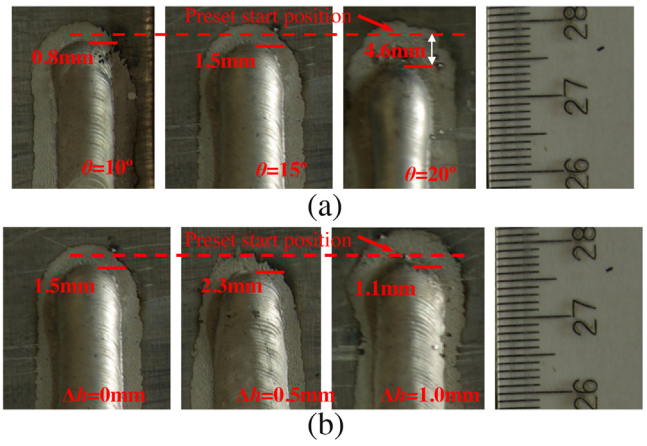

Fig. 3. Effect of (a) θ value and (b) Δh value on start position shift of the weld bead.

3. Results and discussions

3.1. Effect of wire feed manner on weld bead start position

Fig. 3 shows the effects of wire feed manner on layer start position, which is illustrated through designing a group of experiments by taking θ and Δh (h) values as the experimental variables. Fig. 3a shows the start position shifting with θ value (10°, 15° and 20°) under the condition of bridging transfer, and Fig. 3b shows the shift varying with Δh (0, 0.5 mm and 1.0 mm) when wire feed angle is set as 15°.

Fig. 3a indicates that under the bridging transfer mode (where $\Delta h = 0$), the start position varies significantly with wire feed angle, where the shift increases from 0.8 mm to 4.6 mm. In bridging transfer mode, it is reasonable that the wire feed angle actually determines the droplet "landing" position. Increasing the angle shifts the "landing" position away from the arc axes (i.e., preset position). It should be noted that the wire was fed in front of the arc travel direction. Thus the start position shift increases because the wire flying distance in arc zone increases with wire feed angle. In Fig. 3b, start position shift firstly increases from 1.5 mm to 2.3 mm and then decreases to 1.1 mm when increase Δh from 0 to 1.0 mm at θ = 15°. Such regulation of Δh elevates the wire tip so that creates larger gap between the droplet and molten pool surface. This gap allows the droplet to grow larger before transfer and therefore lowers the transfer frequency, which is confirmed by the coarse surface ripples when $\Delta h = 0.5$ mm and 1.0 mm. The large droplet implies prolonged heating of the wire, retraction of which would result in far "landing" position as indicated by $\Delta h = 0.5$ mm. However, as the wire tip was further elevated to $\Delta h = 1.0$ mm, the droplet transfer mode was changed. Instead of "landing", the droplet "flies" into the molten pool forced by the arc. Thus the globular transfer compensates the shift of the start position to some extent.

The results indicate a tendency that a small θ and large Δh would reduce or even eliminate the start position shifting. However, θ and Δh has a significant influence on layer appearance. That is, surface quality is a restriction of θ and Δh variation. The following experiments will be carried out to illustrate the relation between Δh value and the as-deposited layer appearance with the help of high-speed video camera.

3.2. Effect of droplet transfer on layer appearance

The effect of Δh (which denotes the distance variation of wire tip to molten pool surface) on layer appearance was experimentally investigated. Under bridging transfer at wire feed angle 15°, the height h was designed as a reference value and its increment Δh was initially set to 0. When Δh is increased from 0 to 1.0 mm, the wire tip is elevated accordingly, so the droplet transfer mode would change to globular transfer. The effect of droplet transfer on layer appearance was observed with this method. Figs. 4–6 show droplet transfer behavior during one pulse cycle when the wire is elevated with different Δh and their corresponding layer appearance.

Fig. 4 shows bridging transfer, during which, wire was melted in the period of positive polarity continuously. The stable and continuous materials input help to achieve smooth and consistent layer appearance. Increasing h by $\Delta h = 0.5$ mm, gap between wire tip and molten pool surface is increased to 0.5 mm, which allows the droplet to grow larger (almost 1.5 times of the wire diameter) before transfer so as to lower the transfer frequency. Thus the droplet continuously aggregates at wire tip until it contacts the molten pool surface. After it is transferred into the molten pool by surface tension, ridged zones are formed on the layer surface. The ridged zones may be caused by the arc disturbance as shown in Fig. 5 by the right frame, where the arc column becomes tilted by the restraint of the large size droplet. 'Thermal pinch effect' of the arc may be responsible for the tilted arc, in which the large droplet 'cools' the adjacent periphery of the arc column and 'push' the arc column away. Large droplet in globular transfer mode usually makes the deposition process unstable.

Further increasing h by $\Delta h = 1.0$ mm, the large gap between wire tip and molten pool surface makes droplet difficult to transfer. Thus, in the period of positive polarity, the droplet is kept growing and dangling on wire tip, or even spreads back along the wire assisted by the arc force as shown in Fig. 6 by the right frame, where the droplet transfer becomes irregular with spatter occurred. The bulges are enlarged by the lower droplet transfer frequency. Accordingly, surface appearance with humps and hollows is formed.

It is clear that bridging transfer mode makes for smooth and consistent layer appearance, in which both smaller θ and Δh are needed. However, such regulations take risk of start position shift as has been discussed in Section 3.1. Typically, bridging transfer is sensitive to wire feed manner while fixing $\Delta h = 0$. A slight deviation of feeding angle θ would cause wire flexed or punctured through the arc column as shown in Fig. 7, in which, instead of stable melting, the wire tip either strikes directly onto the solid surface of the layer or flies over the molten pool before melting. Thus, it is necessary to construct a model to describe the wire flying and melting condition by considering the variations of feeding angle θ and height adjusting Δh. Thus, an operation window should be drawn for stable wire melting and bridging transfer, according to which displacement compensation would be made at the arc striking position. Mathematical model of wire flying distance in arc zone

Even a tiny variation in θ and Δh would cause distinct start position shifting and undulating surface. For the narrow operation window, it is usually a tedious work to experimentally determine the start position shifting and achieve bridging transfer synchronously. So it is necessary to model the wire molting process, by which wire flying distance in arc zone would be theoretically calculated. Further taking the wire flying distance as a reference, start position shifting could be determined according to

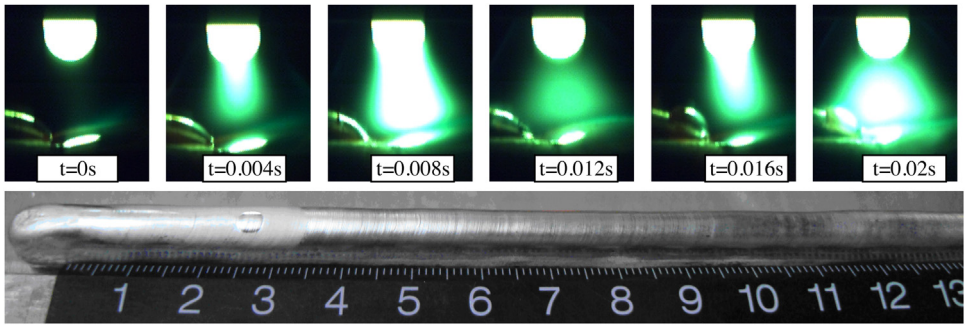

Fig. 4. High-speed images of droplet bridging transfer in one pulse cycle with $\Delta h = 0$ mm and the corresponding macroscopic layer appearance.

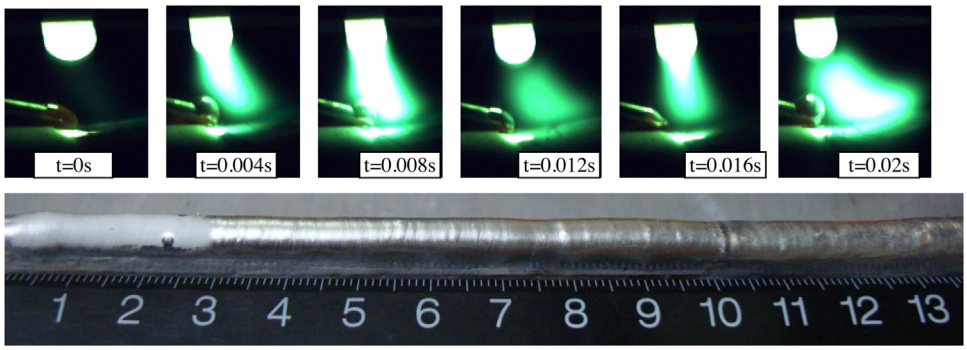

Fig. 5. High-speed images of droplet transfer in one pulse cycle with $\Delta h = 0.5$ mm and the corresponding macroscopic layer appearance.

the droplet "landing" position, and wire feed manner could also be designed to achieve bridging transfer.

At the arc striking position, weld torch moves forward and heat accumulation in molten pool is insufficient. The molten pool is small and shallow, from where heat is extracted rapidly. Temperature gradient at fusion line is large. Now the molten pool is in "cold state", where molten metal is viscous. Especially for the first droplet, it could not flow and solidifies rapidly at the "landing" position. Under the present circumstances, the molten metal could not flow to the projection position of tungsten electrode from the "landing" position. So the position where wire starts to be melted in arc zone is seen as the layer start position. Displacement compensation is determined by calculating the distance from layer start position to tungsten electrode projection.

For thin substrate, a small shadow molt pool would be formed and the layer start position shift may be minished owing to short range flow. That does not have severely negative effects on dealing with the trouble of deposition accuracy because the calculated compensation value is greater than the actual one when regard it as thick substrate. Further machining is usually needed for WAAM because of the poor surface quality, during which overmuch increment can be machined away. From this point of view, the calculated compensation values larger or equal to the actual one are all advisable.

Fig. 8 shows the modeling process of arc shape and heat flux distribution. As Modenesi and Reis (2007) and Janez (2000) pointed out that wire was melted by direct arc heating when flying in arc zone during GTAW process. The arc was regard as point heat source to model the wire melting process. Here it is seen as a space heat source. The longitudinal section shape of electric arc zone is approximated to isosceles trapezoid, and Gaussian distribution is applied to the whole trapezoid zone to describe the heat flux distribution along radius.

Based on the following assumptions, wire feed process could be further simplified.

i Neglecting heat flux disturbance caused by the change of wire flying height when wire is fed at small angle. Heat flux is simplified as a function of the radius of arc seiscrop section. Because wire is fed in a small angle, the height change is very small. Comparing to fusion enthalpy of the wire, the error caused by the height change is negligible.
ii In the modeling process, the differential element at the wire tip is treated as adiabatic while it is flying in arc zone. Because the wire is fed into the arc zone in high speed, the succeeding localized wire flies into arc zone and is melted instantaneously. The continuous heating and melting result in high heat resistance effect. Thus consider the time effect, transient heat conduct along the wire is negligible.
iii The molten pool surface is plane surface at arc striking position.
iv The molten metal aggregates and forms spherical droplet at the wire tip.
v Considering only the gravity and surface tension during wire melting process.

According to the above hypothesis, wire feeding and melting is modeled as the following process.

The process of wire feeding and melting is graphically represented in Fig. 9, in which the wire feeding process is decomposed into a group of continuous flying differential elements with length of "*dl*". The position where wire begins to melt is decided by heat accumulation along the flight trajectory. When heat flux integration along flight trajectory is equal to melting heat, the wire begins to melt into droplets and subsequently land onto the substrate. So the path of integration determines the wire flying distance in the arc zone. The melting heat of the wire with length of *dl* is expressed as

$$Q_m = \int \rho c A \cdot dl \cdot (T_m - T_0) \tag{1}$$

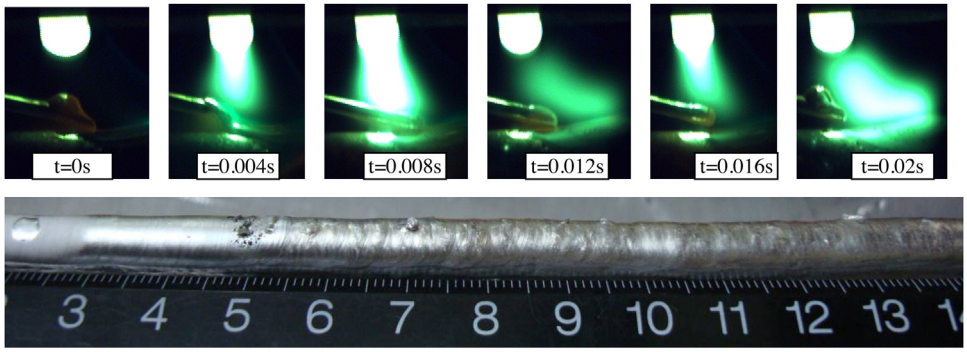

Fig. 6. High-speed images of droplet transfer in one pulse cycle with $\Delta h = 1.0$ mm and the corresponding macroscopic layer appearance.

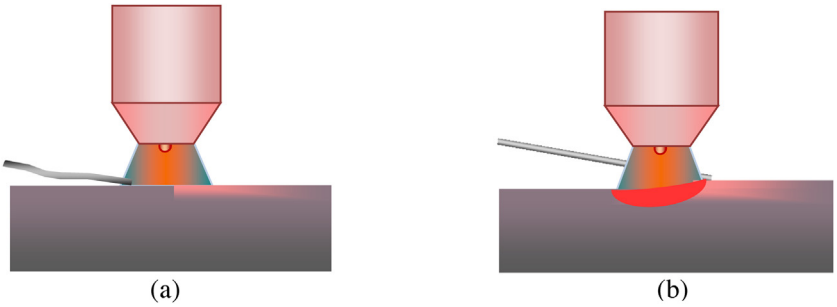

Fig. 7. Phenomena of (a) wire bend and (b) wire fly through arc zone due to un-melted wire.

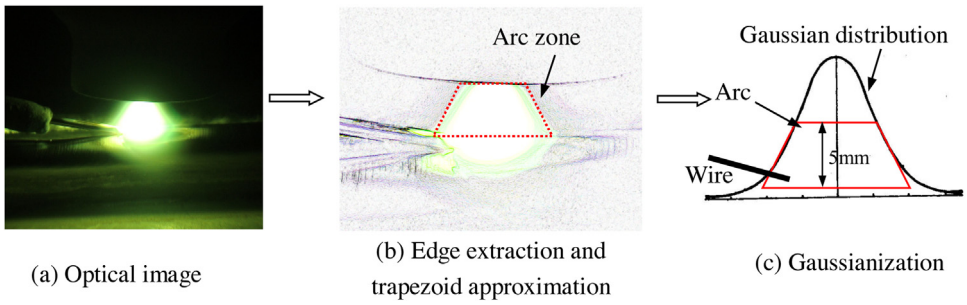

Fig. 8. Modeling process of the electric arc.

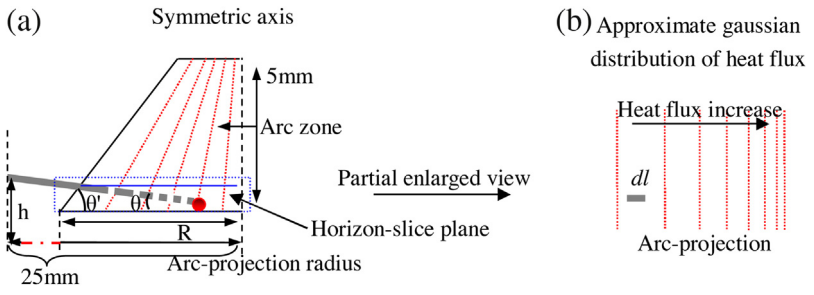

Fig. 9. Schematic of wire feeding and melting (a) and (b) partial enlarged view of dashed box.

where ρ is density, c is specific heat, A is cross section area of the wire, T_m is melting temperature and T_0 is room temperature. Heat flux integration along flight trajectory determines where the wire starts to be melt. Heat flux with Gaussian distribution along radial direction is expressed as

$$q(r) = q_{\max} \cdot \exp(-kr^2) \tag{2}$$

where $q_{\max}$ is the maximum heat flux occurred at the center of heat resource, r is the radial distance to projection of tungsten electrode. k is the concentration coefficient. It is common to know that the effective heating radius varies along with arc length, here taking 95% $q_{\max}$ as the set value to decide the heating radius r(h'), where h' stands for the vertical distance of wire to tungsten electrode at the edge of arc zone. Relation between the concentration coefficient and heating radius is expressed as follow

$$e^{-kr(h')^2} = 0.05 \Rightarrow k = \frac{\ln 20}{r(h')^2} = \frac{3}{r(h')^2} \tag{3}$$

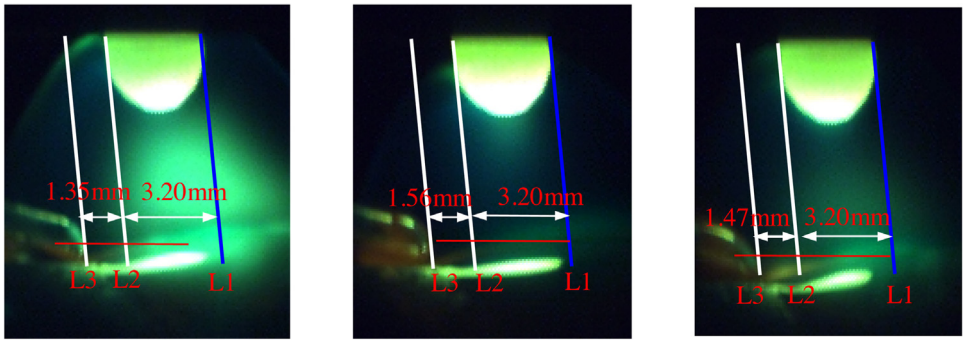

Fig. 10. Three captured photos from high speed video photography in reverse-polarity cycle.

The maximum value of heat flux is

$$q_{\max} = \frac{kp}{\pi} = \frac{3 \cdot \eta UI}{\pi r^2} \tag{4}$$

where p is arc powder, η is heating efficiency, U is effective voltage of welding power supply and I is effective current. In the experiments, arc length is set to a fixed value 5 mm and the other process parameters are unchanged except the wire feeding related parameters. So the arc shape is similar. Base angle θ' of the isosceles trapezoid, as shown in Fig. 9a, is mathematically expressed as

$$\tan\theta' = \frac{5}{R} \tag{5}$$

where R is the heating radius when the arc length is 5 mm. In the experiments, R is a constant value and can be measured in the optical images. Consequently, r and k become a function of h'.

$$r(h') = \frac{h'}{\tan\theta'} = \frac{h'R}{5} \tag{6}$$

Upon substituting Eq. (6) into (3), the following relation is derived.

$$k(h') = \frac{3}{r^2(h')} = \frac{75}{h'^2 \cdot R^2} \tag{7}$$

Eq. (7) does not imply the physical meanings of k. It is just a mathematic formula to show the relation between concentration coefficient and arc shape. Half of the surface area of cylindrical welding wire is heated by arc, so heating surface area of wire is

$$s = \int \pi r_w v_w \cdot dl \tag{8}$$

where r_w is welding wire radius. v_w is wire feed speed. In unit time, heat absorption of differential elemental dl is expressed as

$$Q_i = q(h') \cdot s = \frac{3}{R^2} \cdot \frac{25}{h'^2} \cdot \eta UI \cdot \exp(-\frac{75r^2}{h'^2 \cdot R^2}) \cdot \int r_w v_w \cdot dl \tag{9}$$

Considering the flying distance r(h')-r, integrator of Q_i is equal to Eq. (1), total heat absorbing during wire flying in arc zone is

$$Q = \int_0^{r(h')-r} Q_i dl = \rho cA \cdot (T_m - T_0) \cdot dl = Q_m \tag{10}$$

Substituting $dl = v_w \cdot dt$ into Eq. (10), the follow equation is obtained.

$$Q = \int_0^t \frac{3}{R^2} \cdot \frac{25}{h'^2} \cdot \eta UI \cdot \exp(-\frac{75(v_w t)^2}{h'^2 \cdot R^2}) \cdot r_w \cdot dt = \rho cA \cdot (T_m - T_0) \tag{11}$$

By integrating the left-hand side of Eq. (11), equation in integral form can be obtained.

$$Q = \frac{5}{2}\eta UI \cdot \frac{r_w}{Rh'} \cdot \sqrt{\pi} \cdot \frac{\sqrt{3}}{v_w} \cdot erf(\frac{5}{h'} \cdot \frac{\sqrt{3}v_w}{R} t) = \rho cA \cdot (T_m - T_0) \tag{12}$$

when h' = 5 mm, R is measured from the optical image and its value is 7 mm. Substitute these values into Eq. (12), so

$$Q = \frac{1}{2R}\eta UI \cdot r_w \cdot \sqrt{\pi} \cdot \frac{\sqrt{3}}{v_w} \cdot erf(\frac{\sqrt{3}v_w}{R} t) = \rho cA \cdot (T_m - T_0) \tag{13}$$

In a limiting case that the wire is fed at a low angle and almost parallel to the substrate, the wire flying distance in arc zone can be calculated from Eq. (13). Taking the error function as an entire variable, the value is calculated by substituting the process parameters into this equation, in which the parameters used for calculation is listed in Table 2. That is

$$erf\ (\frac{\sqrt{3}v_w}{R} t) = 0.78 \tag{14}$$

In the experimental conditions, wire flying distance in arc zone is calculated as 3.52 mm by referring to the error function table. The limitation of error function is 1.0, so the maximum wire flying distance is 4.05 mm.

To verify the developed model, the following experiments are conducted, in which the wire is fed at low angle 8°, and the vertical distance of wire to tungsten electrode is 5 mm. The horizontal distance of melting wire tip to axis of tungsten electrode is measured in high speed photographs by taking diameter of tungsten electrode as reference. Fig. 10 shows a collection of photos captured from high speed video photography with an interval of five pulse cycles.

Lines L1 and L2 are drawn as the contours of tungsten electrode. L3, in parallel, is drawn through the wire tip. Diameter of tungsten electrode is 3.2 mm, so distance of L1–L2 is regarded as 3.2 mm, which is taken as a scale to measure the distance of melting wire tip to the axis of tungsten electrode. The measured value is in the range of 2.95 mm–3.16 mm. So wire flying distance is in the range of 3.84 mm–4.05 mm, of which the average value is 3.94 mm. The experimental value is slightly larger than the calculated one 3.52 mm, which may be caused by the retained molten metal at the wire tip due to surface tension. If the results are in a mean error of 0.4 mm, the calculated value would be in good agreement with the experimental results.

3.3. Optimizing control strategy of wire feed manner

The wire flying distance calculated by Eq. (12) with varied h' is schematically illustrated in Fig. 11. When vertical distance of wire tip to tungsten electrode is changed from 5 mm to 3 mm, droplet landing position only has a little change, about 0.4 mm, which allows a flexible design of wire feeding to achieve bridging transfer. However, the distance from melting wire tip to molten pool surface should not larger than the maximum diameter of spherical droplet, or the droplet is transferred into molten pool in globular transfer mode.

Table 2
Data used for calculating wire flying distance in arc zone.

Process parameters (Unit)	Notation	Value	Process parameters (Unit)	Notation	value
heat efficiency	η	0.3	Density (g/cm^3)	ρ	2.7
Voltage (V)	U	11.6	Specific heat capacity (J/g k)	c	0.88
Current (A)	I	160	Melting point (k)	T_m	933.15
Wire radius (mm)	r_w	0.6	Room temperature (k)	T_0	293.15
Wire feed speed (m/min)	v_w	2.0			

Note: The value of heat efficiency is set according to Cantin and Francis (2005)'s research result.

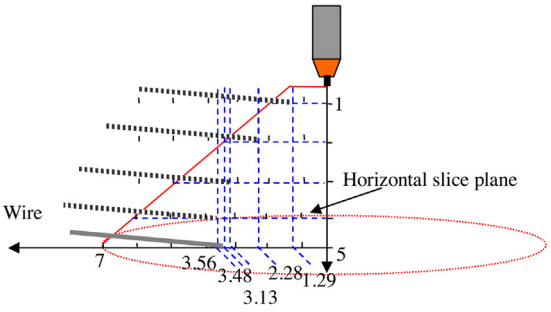

Fig. 11. Schematic illustration of wire flying distance in arc zone and droplet dripping location with varying h′ value when v_w = 2 m/min.

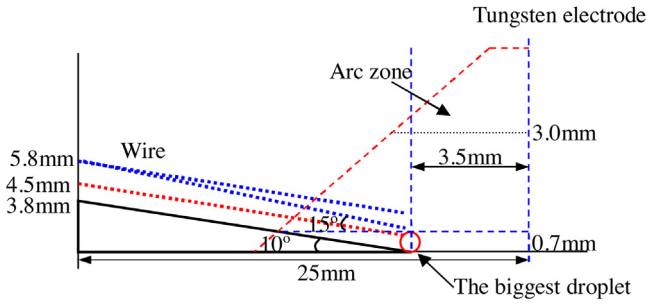

Fig. 12. Geometric relationship of wire feed manner to achieve bridging transfer.

Based on the hypothesis, maximum diameter of spherical droplet can be estimated using the follow formula according to Arif et al. (2008) and Doodman Tipi et al. (2015).

$$2\pi r_w \gamma = \frac{4}{3}\pi r_d^3 \rho g \tag{15}$$

where, γ is surface tension coefficient and r_d is radius of droplet. Goicoechea et al. (1992)'s research showed that surface tension coefficient γ of Al-5wt% Mg alloy is 0.798 N m^{-1} at 973k, so the r_d value is approximately equal to 0.7 mm, which is confirmed by the surface appearance observation showed in Figs. 4, 5 and 6. When Δh is less than or equal to 0.5 mm, droplet transfer mode does not change, so is the transfer frequency. When Δh equals to 1.0 mm what is larger than the calculated r_d value 0.7 mm, the droplet transfer mode changes to globular transfer and deposition process becomes instable, so undulated surface appearance is observed.

When wire is fed at low angle, i.e., vertical distance between wire tip to tungsten electrode falls in the range of 3.0 mm–5.0 mm, bridging transfer is easily achieved through wire translation movement or rotation movement. Because they only results in a little change in wire flying distance, about 0.4 mm, the displacement compensation for layer start position shift could be set as constant value under the deposition condition. Using this displacement compensation method, layer size precision and surface appearance could be jointly improved. In verification experiments, wire feed angle is set as 10°, the translation or rotation movement range changes to 3.8 mm–5.8 mm. Fig. 12 shows the methods of adjusting wire feed manner to achieve bridging transfer while keeps the same displacement compensation.

When wire feed angle is 10°, h will not exceed 4.5 mm. Thus, the welding wire translation movement (i.e. changing h value) and rotation movement (i.e. changing θ value) will not change wire flying distance in arc zone and droplet transfer mode. The displacement compensation is 3.5 mm. However, if h is adjusted in the range of 4.5 mm ~ 5.8 mm, to ensure bridging transfer, the two movements are needed jointly to keep the distance of melting wire tip to molten pool surface not more than 0.7 mm. Using the developed method, it is easy to fulfill bridging transfer and overcome "gap" defect by means of displacement compensation. Fig. 13 shows the optimization result.

when Δh is less than 0.5 mm at wire feed angle 15° as indicated in Fig. 3, the calculated start position matches well with the experimental results. Increasing Δh to 1.0 mm, error is aroused because the model is developed basing on the hypothesis that molten metal could not be retained at the wire tip. When Δh is increased to 0.5 mm or larger, retained molten metal was observed at the wire tip in the high-speed images, as shown in Figs. 6 and 7, which consequently increase the wire flying distance. In addition, the theoretical model only considers the first droplet landing position. In fact, the layer is formed by several droplets at the start position and the molten metal spreading on the substrate further reduces the start position shift. So the calculated displacement compensation is slightly larger than the actual one.

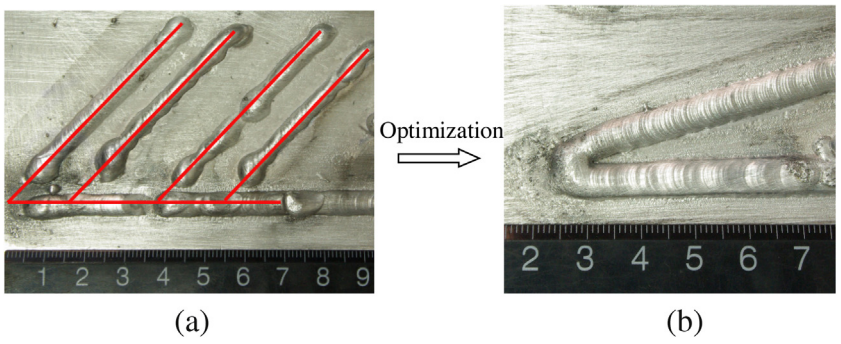

Fig. 13. comparing (a) the as-deposited cross structure without dimension correction with (b) layer size correction via the proposed displacement compensation value.

4. Conclusions

(1) When wire feed angle is increased from 10° to 20°, start position shift increases from 0.8 mm to 4.6 mm. When the vertical distance of melting wire tip to molten pool surface (Δh) is increased from 0 to 1.0 mm, start position shift increases from 1.5 mm to 2.4 mm firstly, and then decreases to 1.1 mm.
(2) An optimizing of wire feed manner is developed by considering both the layer size precision and layer surface appearance. Wire is fed with small angle 10° and h value 3.8 mm could ensure smooth layer appearance. Displacement compensation value 3.5 mm is designed to offset the start position shift by calculating wire flying distance in arc zone.
(3) When vertical distance of melting wire tip to tungsten electrode is varied within 2.0 mm, the droplet landing position changes within 0.4 mm. That allows translation or rotation movement to achieve bridging transfer.
(4) In the verification experiment, the vertical distance of melting wire tip to tungsten electrode is set to 5 mm and displacement compensation value is set to 3.5 mm, good acute-angle shape is deposited.

Acknowledgements

This work was supported by the National Natural Science Foundation of China (Grant No. 51575451) and the Research Fund of the State Key Laboratory of Solidification Processing (NWPU), China (Grant No. 109-QP-2014).

References

Arif, N., Lee, J.H., Yoo, C.D., 2008. Modelling of globular transfer considering momentum flux in GMAW. J. Phys. Appl. Phys. 41, 1–6.
Baufeld, B., der Biest, O.V., Gault, R., 2009. Additive manufacturing of Ti–6Al–4V components by shaped metal deposition: microstructure and mechanical properties. Int. Conf. Mater. Adv. Technol. 31 (Supplement 1), s106–s111.
Baufeld, B., Brandl, E., der Biest, O.V., 2011. Wire based additive layer manufacturing: comparison of microstructure and mechanical properties of Ti6Al4V components fabricated by laser-beam deposition and shaped metal deposition. J. Mater. Process. Technol. 211, 1146–1158.
Cantin, G.M.D., Francis, J.A., 2005. Arc power and efficiency in gas tungsten arc welding of aluminium. Sci. Technol. Weld. Joining 10, 200–210.
Doodman Tipi, A.R., Hosseini Sani, S.K., Pariz, N., 2015. Frequency control of the drop detachment in the automatic GMAW process. J. Mater. Process. Technol. 216, 248–259.
Goicoechea, J., Garcia-Cordovilla, A., Louis, E., Pamies, A., 1992. Surface tension of binary and ternary aluminium alloys of the systems Al-Si-Mg and Al-Zn-Mg. J. Mater. Sci. 27, 5247–5252.
Janez, T., 2000. Mathematical modeling of melting rate in twin-wire welding. J. Mater. Process. Technol. 100, 250–256.
Modenesi, P.J., Reis, R.I., 2007. A model for melting rate phenomena in GMA welding. J. Mater. Process. Technol. 189, 199–205.
Ouyang, J.H., Wang, H., Kovacevic, R., 2002. Rapid protyping of 5356-aluminum alloy based on variable polarity gas tungsten arc welding: process control and microstructure. Mater. Manuf. Process. 17, 103–124.
Wang, H., Kovacevic, R., 2001. Rapid prototyping based on variable polarity gas tungsten arc welding for a 5356 aluminium alloy. Proc. Inst. Mech. Eng. B: J. Eng. 215, 1519–1527.
Wang, F.D., Williams, S., Colegrove, P., Antonysamy, A.A., 2013. Microstructure and mechanical properties of wire and arc additive manufactured Ti-6Al-4V. Metall. Mater. Trans. A 44A, 968–977.